AGU PUBLICATIONS

JGR

Journal of Geophysical Research: Atmospheres

RESEARCH ARTICLE

10.1002/2016JD025559

Key Points:

- Three frequency ranges were established (0.5-2, 2-8, and 8-100 1/day) in temporal spectra for wind speed and wave height with various spectral slopes
- Spectral slopes depend on location of the considered point to the equator
- Direct relations between spectra for wind, pressure, and wave height were derived from the Navier-Stokes equations

Correspondence to:
V. G. Polnikov,
polnikov@mail.ru

Citation:
Polnikov, V. G., and F. A. Pogarskiy (2017), Spectra of long-term series for wind speed and wave height in the Indian Ocean area, *J. Geophys. Res. Atmos.*, *122*, 104–120, doi:10.1002/2016JD025559.

Received 22 JUN 2016
Accepted 18 NOV 2016
Accepted article online 23 NOV 2016
Published online 9 JAN 2017

Spectra of long-term series for wind speed and wave height in the Indian Ocean area

V. G. Polnikov[1] and **F. A. Pogarskiy**[1]

[1]Obukhov Institute of Atmospheric Physics, Russian Academy of Sciences, Moscow, Russia

Abstract The spectra of long-term series of wind velocity and significant wave height were built in two domains of variability scales: from 1 day to 1 year (D1) and from 1 year to 15 years (D2). Surface wind data from the ERA-Interim reanalysis in the Indian Ocean area for the period of 1979–2015 years, and wave heights simulated with the improved WAM model, were used for this purpose. In order to study the spatial variability of the spectral shapes, spectra of wind speed and wave height were calculated at two sections located along the meridians and three sections located along latitudes with a step of 3°. For the D1 domain, the existence of three ranges of variability scales (R1, R2, and R3) are shown in which both types of spectra have the well-defined and visibly different power-like slopes varying in dependence on the offset from the equator. The Navier-Stokes equations were analyzed in order to design a theoretical interpretation of the spectral shapes features found in the D1 domain. For the D2 domain, no unified system of isolated frequencies has been revealed, which is expected for the entire Indian Ocean. Among the set of selected periods, the most stable one is the variability period of around 5.5 years. Results presented in this work are discussed.

1. Introduction

A great number of papers have been dedicated to the study of spectral characteristics for temporal meteorological fluctuations [e.g., *Monin and Sonechkin*, 2005; *Hamilton et al*. 2008; *Tsuchiya et al*., 2011; *Skamarock et al*., 2014, and references therein]. The main reason for this interest lies in the fact that an analysis of spectral shapes for geophysical temporal series is one of the efficient tools to investigate the dynamics of natural processes. For this purpose, data of both long-term measurements [*Monin and Sonechkin*, 2005; *Tsuchiya et al*., 2011] and numerical simulations are utilized [*Hamilton et al*., 2008; *Skamarock et al*., 2014]. These data could be obtained by various methods: contact measurements [*Tsuchiya et al*., 2011], remote sensing [*Young et al*., 2011, 2013], aircraft sensing [*Skamarock et al*., 2014], sensing from vessels [*Gulev and Grigorieva*, 2006], buoys [*Polnikov and Pogarskii*, 2013], drifters [*Golitsyn*, 2013], and many others. The simulated series, subjected to spectral analysis, is usually created by numerical models of different complexity [*Hamilton et al*., 2008; *Tsuchiya et al*., 2011; *Skamarock et al*., 2014]. The diversity of these approaches is dictated by a need to determine new empirical relationships [*Monin and Sonechkin*, 2005; *Tsuchiya et al*., 2011] or by a quality control of reproduction of known empirical relationships by the numerical simulations [*Skamarock et al*., 2014; *Serykh and Sonechkin*, 2015].

It is important to note the two physical differences in the spectral estimations: spectra can be both spatial, $S(\mathbf{k})$, i.e., built in the wave vector space, $\mathbf{k} = (k_x, k_y, k_z)$, [*Hamilton et al*., 2008; *Skamarock et al*., 2014] and temporal, $S(\omega)$, i.e., done in the frequency space, ω [*Monin and Sonechkin*, 2005; *Tsuchiya et al*., 2011; *Polnikov and Pogarskii*, 2013]. Calculations of spatial spectra are widely used to test various models describing the formation of turbulence in the fluid, as far as the models of turbulence are built in the k space, mainly [*Monin and Yaglom* 1971]. This approach is based on using moving instruments: aircraft, satellites, ships, and drifters [*Golitsyn*, 2013; *Skamarock et al*., 2014]. Frequency spectra, on the contrary, are based on the time series obtained at fixed points [*Monin and Sonechkin*, 2005; *Tsuchiya et al*., 2011; *Polnikov and Pogarskii*, 2013], which is convenient for a quality control of numerical models and understanding the physics of natural phenomena.

A significant difference in such kind of studies consists of a choice of the considered variability scales: from centimeters to several hundred kilometers for spatial spectra [*Hamilton et al*., 2008; *Skamarock et al*., 2014] and from a fraction of a second to tens of years or more for temporal spectra [*Monin and Sonechkin*, 2005; *Tsuchiya et al*., 2011; *Pogarskii et al*., 2012].

Our research is related to the investigation of the temporal spectra on the scales of variability from half-a-day to decades, calculated for long-term wind speed and wave heights series collected at numerous locations in the

Indian Ocean. Therefore, we are interested in the temporal variability of meteorological quantities at selected points of a water area, including a spatial variability of temporal spectra for quantities under consideration.

Works of such kind are performed by various research groups [see *Monin and Sonechkin*, 2005; *Tsuchiya et al*., 2011, and references therein]. Over the last few years, similar studies were performed by the present authors [*Pogarskii et al*., 2012; *Polnikov and Pogarskii*, 2013]. In these papers, it was reported that the spectral shape $S(\omega)$ of long-term series is stable through the variability of scales from one day to 1 year, and it has a number of features. In *Tsuchiya et al*. [2011] such spectra are referred to as "universal." In contrast to these results, we have found that the spectra stability depends on the length of series only, with the proviso that a series cover periods more than 3–5 years. Herewith, the shapes of spectra for all geophysical quantities depend strongly on the offset of the considered point of position from the equator. That means that these spectra are not universal. Parameters characterizing spectral shapes of various meteorological variables are significantly different [*Tsuchiya et al*., 2011; *Pogarskii et al*., 2012].

Nevertheless, all temporal spectra of such variables have many similar features in the domain of scales from 1 day to 1 year, denoted here as D1. For example, in the observations of series spectra of surface temperature, pressure, and wind-velocity components, measured at the Japanese islands [*Tsuchiya et al*., 2011], the existence of two ranges of variability periods (designated here as R1 and R2) with significantly different power-like frequency dependence of the type $S(\omega) \propto \omega^{-\alpha}$ was found. According to *Tsuchiya et al*. [2011], in the R1 range of periods, covering scales from 1 to 6–8 days, the spectra slopes correspond to value $\alpha > 1.5$–2, which vary considerably for various physical quantities. On the larger scales of variability R2, covering periods from 10 to 100 days, the spectra of all quantities are characterized by very small slopes ($\alpha \ll 1$).

Similar results were obtained in *Pogarskii et al*. [2012], where the series of wind data from National Centers for Environmental Prediction-reanalysis and simulated wind wave data in the Indian Ocean (IO) area were used, covering a period of 1998–2009. In the present paper, the same results were obtained (based on other data, but with a much more complicated system of stable spectral slopes in the D1 domain of scales).

A fairly complete phenomenological description of such kind of features for spectral shapes was carried out in [*Tsuchiya et al*., 2011]. A more schematic description of these was done in *Pogarskii et al*. [2012]. However, spectra features have not yet acquired their clear physical explanation. In this paper, we offer a detailed description of the detected features of the spectra for wind $S_U(\omega)$ and wave height $S_{H_s}(\omega)$, calculated with 35 year data series, and present a version of their physical interpretation by involvement of the fundamental equations of hydrodynamics.

First, in the case of D1 scales of variability, we clarify the causes of partitioning the entire geography area into two latitudinal zones, Z1 and Z2, where different spectral shapes $S_U(\omega)$ and $S_{H_s}(\omega)$ are observed. Second, we describe possible physical mechanisms regulating the shapes of these spectra in different frequency bands (designated as the R1, R2, and R3 ranges). Third, we justify theoretically a strong relationship between spectral shapes $S_{H_s}(\omega)$ and $S_U(\omega)$, taking place at the same fixed points.

The larger scales of variability, from 1 year to 15–20 years, which we denote as the D2 domain of periods, should be considered separately, as far as this domain of scales corresponds to the climate and global variability [*Monin and Sonechkin*, 2005]. This domain of scales was not considered in papers [*Tsuchiya et al*., 2011; *Pogarskii et al*., 2012]. However, the variability of wind and temperature fields on such scales was intensively studied by other authors in papers devoted to the analysis of the global cycles of atmospheric circulation on climatic scales (see, numerous references in monography [*Monin and Sonechkin*, 2005], notably, the papers *Lorenz* [1991], *Lovenjoy and Schertzer* [1985], *Govindau et al*. [2002], among others). Recently, it was shown [*Serykh and Sonechkin*, 2015] that for the D2 domain of scales, the spectra of surface temperature, obtained with a special spatial-temporal averaging of initial reanalysis series, represent a discrete set of isolated peak frequencies, which is determined by the global geophysical and astronomical parameters of the Earth [*Monin and Sonechkin*, 2005]. Naturally, for a series of wind and waves in the IO area considered here, a great interest is to clarify the existence of the similar features in our spectra estimations. To this extent, in this paper, we deliver the results of wind speed and wave height spectra estimations in the D2 domain of scales and present the initial analysis.

The structure of the work is as follows: all scales of variability are assigned into two domains: D1, covering the periods of variability from a day to a year, and D2, covering the periods from 1 to 20 years. First, we describe and analyze the results for D1 domain, while the results and proper analysis for the D2 domain are presented after the summary of results for the D1 domain. A brief overview of the data and the method of processing are given in section 2. In section 3, all diversity of features for the frequency spectra of wind speed $S_U(\omega)$ and significant wave height $S_{H_s}(\omega)$ are given in detail for the D1 domain. Additionally, we describe a number of important, though subsidiary (technical) features of temporal spectra, which we use in the further analysis of empirical results. The corresponding dynamic equations, which we use to get a theoretical interpretation of the results, are presented in section 4. Theoretical relationships between spectra $S_U(\omega)$ and $S_{H_s}(\omega)$ are presented also. Section 5 contains the detailed clarification of the proposed interpretation of the D1 domain spectra features. The spectra estimations' results for the D2 domain and proper analysis are given in section 6. The final results of the work are summarized in section 7.

2. Input Data, Methods of Processing, and Accuracy

The 6-hourly surface wind field $U(x, y, t)$ was taken from the ERA-Interim reanalysis [*Berrisford et al*., 2011] for the period of 1979–2015 years in the IO area for the grid 1.5 x 1.5°. Based on these data, the field of significant wind-wave height, $H_S(x, y, t)$ was calculated with the same spatial and temporal resolution and geographic area. The wind wave model WAM-4 [*The WAMDI Group*, 1988] was used. Physical parameterization of the model has been modified earlier to improve its accuracy [*Polnikov*, 2005; *Samiksha et al*., 2015].

Since the issue of data preparation and quality verification has been discussed in the literature [see *Pogarskii et al*., 2012, and references therein], we do not dwell on this point. Note only that the both types of data correlate well with the buoy observations, and RMS errors are 10% and 15% for wind speed and wave height, respectively [*Polnikov*, 2005; *Samiksha et al*., 2015]. As shown in *Polnikov and Pogarskii* [2013], this provides a good correspondence between spectral shapes for $S_U(\omega)$ and $S_{H_s}(\omega)$, obtained from both the field and model data.

To detect the spatial variability of spectral shapes $S_U(\omega)$ and $S_{H_s}(\omega)$, the spectral analysis was performed for numerous positions (more than 100) in the IO, located at two meridional sections along 63°E and 90°E longitudes and three zonal sections along 0°N, 9°S, and 42°S latitudes (Figure 1).

The choice of the method for spectral analysis, effectiveness, and accuracy assessment has been discussed in *Polnikov* [1985, and references therein]. As follows from the recommendations of *Polnikov* [1985], the autoregression (AR) method has been used. We have used the AR of the 1500 order, which corresponds to frequencies in the D1 domain for our series, with more than 54,000 points at our disposal. The degrees of freedom number were about 40. In such a case, the confidence intervals are about 30–40%, or 10–15% in the logarithmic coordinates (Figures 2 and 3). Such accuracy of spectral estimations allows a definition of the sought spectra slopes, and, evidently, of the isolated scales of variability, defined by spectra peaks. Thus, all quantitative estimates in the D1 domain have an error not exceeding 10–15%.

The series with 15 day averaging was used for calculating spectra in the D2 domain. The AR order was 240, and the degrees of freedom number was about 4. Therefore, the spectra in the D2 domain have confidence intervals of about 100% in the logarithmic coordinates. These estimations justify accurate detection of the isolated frequencies only, which was the purpose of such calculations.

3. Empirical Features of the Spectral Shapes in the D1 Domain of Scales

To demonstrate the spatial dependence of spectral shapes of $S_U(\omega)$ and $S_{H_s}(\omega)$, it is sufficient to produce the consolidated image of the spectra for meridional section 63°E (Figures 2 and 3). Results for meridian 90°E show the similar pattern. Herewith, the zonal dependence of shapes for spectra $S_U(\omega)$ and $S_{H_s}(\omega)$ (for all zonal sections) is represented by a changing of the annual and diurnal peaks intensity only. These peaks and their multiple harmonics have the well-known explanations, and they are not analyzed further. Note only that the intensity of diurnal peaks decreases with the analyzed point shifting from west to east, as well as from north to south (when crossing the equator). Obviously, this decrease is due to the corresponding increase of the cyclonic activity in the studied area because cyclones make a lowering of the relative intensity of diurnal variability of the wind and wavefields.

For our purposes, the values of the RMS slopes of the spectra, which are noticeably manifested in different parts of the frequency range, are of the main interest. A generalized description of these spectral shape features, starting from spectra for wind speed $S_U(\omega)$ (Figure 2), can be presented as follows.

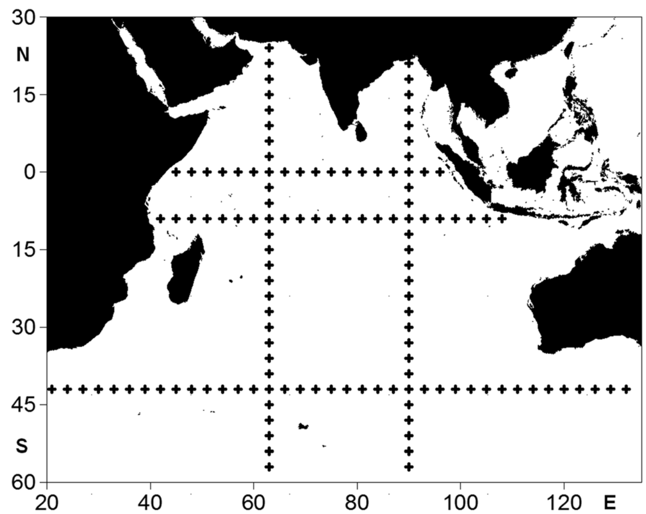

Figure 1. Sites in the IO, selected for the spectra estimation (two longitudinal and three latitudinal sections on the 3 × 3° grid).

3.1. Features of Spectral Shapes for $S_U(\omega)$

First, as seen in Figure 2, the spectral shapes depend essentially on the analyzed point location relative to the equator. Therefore, it is appropriate to introduce a spatial partition of the area into two zones: the near-equatorial latitudinal zone, Z1, and the off-equatorial zone, Z2.

By successive spectra calculations at all points along the meridians sections 63°E and 90°E, we have found that the Z1 zone covers the latitude stripe about [15°N–15°S]. In this zone, in reference to Figure 2, one can distinguish three types of spectral slopes, which we identify as the three features of spectral shapes of $S_U(\omega)$. We denote these features as Z1–U1, Z1–U2, and Z1–U3, corresponding to increasing periods. Empirical description of the features is initiated from the high-frequency feature, Z1–U1.

The feature Z1–U1 is displayed in a very narrow and the most high-frequency bandwidth corresponding to the range of periods from half-a-day to 2 days (denoted here as the first range of periods, R1). Here the slope of spectra $S_U(\omega)$ is close to the decay law "−2."

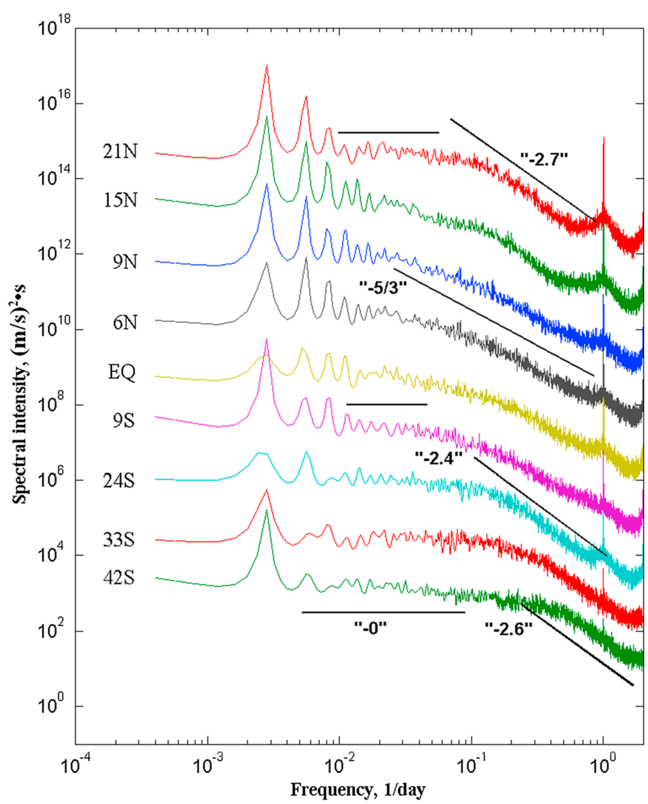

Figure 2. Spectra for wind speed $S_U(\omega)$ at nine points along the 63°E section (spectra are shifted up by a factor of 30). Straight lines show the fixed slopes with power factors in quotes.

The feature Z1–U2 is displayed in a rather large band corresponding to periods from 1–2 days to 30–50 days (the range of periods R2). In the R2 range, the slope of the spectra is close to the law "−5/3." It is the most characteristic feature of the wind speed spectra in the Z1 zone.

The feature Z1–U3 is displayed in the most long-period part of the D1 domain, located in the periods' range of 30–50 to 100–150 days (the R3 range). In this range, the RMS spectral slope becomes very small, designated as the law "−0" and referred to as "the spectral shelf" or "the white noise spectrum."

The sizes of the R1, R2, and R3 period ranges are not fixed, due to the natural variability of the processes considered. For this reason, we do not pay attention to the quantitative characteristics of the R1, R2, and R3 ranges, fixing their existence and number only. The adopted classification of the period ranges will be used for the latitudinal zone Z2, as well.

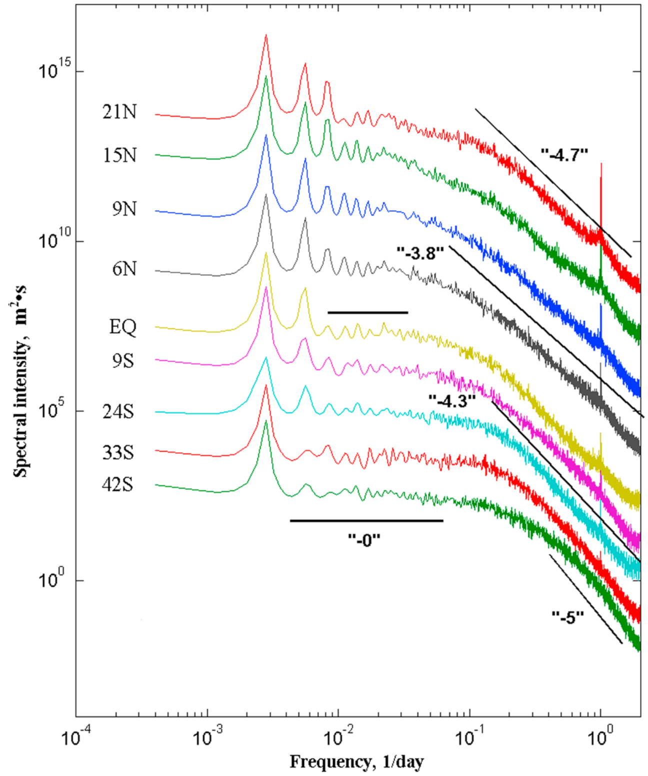

Figure 3. Spectra for significant wave height $S_{H_s}(\omega)$ at nine points along the 63°E section. For legend, see Figure 3.

In the Z2 zone, the shapes of spectra $S_U(\omega)$ and sizes of the equivalent R1, R2, and R3 ranges differ significantly. The proper change of indexing spectral shapes features is done by replacing index Z1 to Z2.

The feature Z2–U1 is displayed in the range from 1 to 6 days (extended equivalent of the R1 periods' range), where the spectral slope is reaching values "-2.6 ± 0.2."

The feature Z2–U2 is displayed in a relatively small range of periods from 3–5 to 8–10 days, when the spectral slope is rapidly changing. In this range, it is difficult to specify a selected spectral slope; however, this range could be identified as the equivalent of R2 range.

The feature Z2–U3 appears as the spectral shelf. This feature is similar to that in the Z1 zone, but in the Z2 zone, it is expressed in a stronger manner. Namely, in a large-frequency band corresponding to the range of periods from 10 to 150 days (the equivalent of extended R3 range), the spectral slope of $S_U(\omega)$ is close to -0 law.

As seen from the empirical description, the spatial variability of spectral shape for $S_U(\omega)$ (in this case, latitudinal variability) is well expressed. However, it is not as simple as it was presented earlier in [*Tsuchiya et al.*, 2011; *Pogarskii et al.*, 2012].

3.2. Features of Spectral Shapes for $S_{H_s}(\omega)$

First, note that a curve-to-curve comparison between Figure 2 and Figure 3 shows a strong relationship between spectral shapes for wind-wave height $S_{H_s}(\omega)$ and wind-velocity $S_U(\omega)$ at the points with the same spatial coordinates. Basically, such a relationship does not assume a separate classification feature for the wave height spectra. However, at a stage of the spectral shapes empirical description, such an independent identification is necessary. For this purpose, we retain the usage of the above designations, postponing the fact of the strong relationship between spectral shapes $S_{H_s}(\omega)$ and $S_U(\omega)$ until a further theoretical justification.

The feature Z1–H1 of spectra $S_{H_s}(\omega)$ is displayed in the narrow range of periods, from half-a-day to 1–2 days (the equivalent of R1 range), where the decay law of wave spectrum is close "-4" (it is the steepest slope in the zone Z1).

The feature Z1–H2 is displayed in the wide frequency band, corresponding to periods from a few to several 10 days (the equivalent of R2 range), in which the well-expressed decay law is of the order "$-(3.7 \pm 0.2)$." Herewith, in the low-frequency part of the R2 range, there is a subrange of scales from 5 to 10–20 days, in which the spectral slope is of the order of "-1." Despite small size of the subrange, the slope is evident and relatively stable. Further, such a feature will be denoted as Z1–H2a.

The feature Z1–H3 takes place in the range of periods from 20–30 to 100–150 days (the equivalent of range R3). In this range, the RMS spectral slope has the very weak dependence on frequency, identified as the law -0.

In the off-equatorial zone, the shapes of spectra $S_{H_s}(\omega)$ have the following three features.

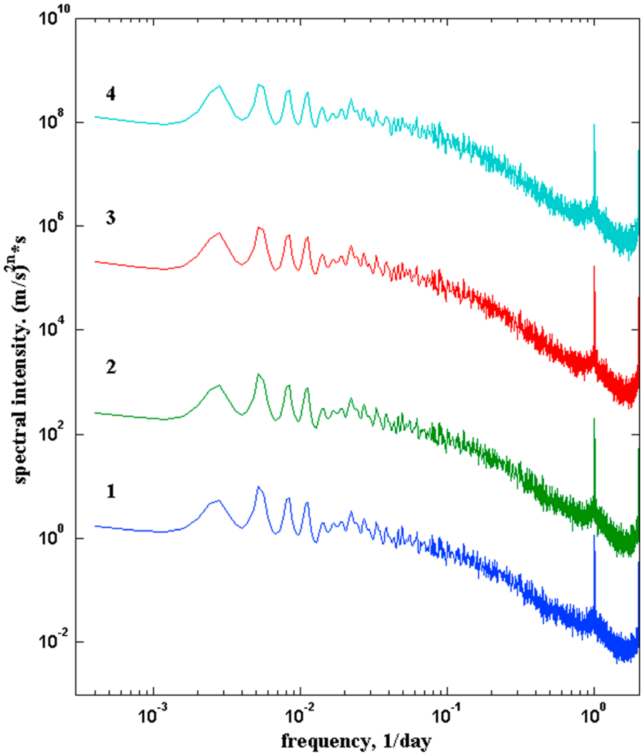

Figure 4. Spectra for series of the wind speed at the point (0°N, 63°E), taken to different powers $U^n(t)$. Spectra are shifted up by a factor of 10. Line 1 corresponds to power $n = ½$; line 2 to $n = 1$; line 3 to $n = 2$; and line 4 to $n = 3$.

1. The feature Z2–H1 is displayed in the fairly wide frequency band corresponding to the periods range from a few to 6–8 days (the equivalent of extended R1 range of periods), where spectra $S_{Hs}(\omega)$ have the steepest slopes in the zone Z2, reaching values "-4.7 ± 0.3."
2. The feature Z2–H2 is realized in the narrow band corresponding to periods from 6–8 to 10–20 days (the equivalent of R2 range), where the spectral slopes change rapidly. Herewith, in the R2 range, there is a visible slope in $S_{Hs}(\omega)$ with the decay law of the order of -1. Apparently, it reflects the weak slopes of spectra $S_U(\omega)$, taking place in the transient R2 range of periods.
3. The feature Z2–H3 is completely analogous to feature Z2–U3 for the wind spectra, having the well-expressed "spectral shelf" like that in the zone Z1 but much more pronounced in the zone Z2. Namely, in the wide frequency band corresponding to the range of periods from 10 to 150 days (the extended R3 range of periods), the spectral slopes for $S_{Hs}(\omega)$ are close to the -0 law.

3.3. Technical Features of the Spectral Shapes

For further analysis, the following are also required: the relationships (a) between spectra for the original and "powered" series (see section 3.3.1), (b) between spectra for wind-velocity components and wind magnitude (section 3.3.2), (c) between spectra of initial and "filtered" geophysical series (section 3.3.3). Therefore, to complete the spectra features description and clarify their further analysis, the auxiliary (technical) properties of spectra for arbitrary random series should be specifically provided.

3.3.1. The Spectra of Powered Series

Such series means that each item of the original series is taken to a certain power. For example, for a constant-sign series, alike the wind-velocity magnitude, $U(t)$, the powered series are the following: $U^{1/2}(t)$, $U^2(t)$, and $U^3(t)$. We need to know how the spectra of such series are related. In short, the results are as follows.

Empirically, it was found that the spectra of powered series have similar shapes shown in Figure 4. The relation coefficients for powered spectra are proportional to the proper power of the variance for original series. If the spectrum for $U(t)$ assumes the form

$$S_U(\omega) = S_0 F(\omega), \tag{1}$$

where S_0 is the variance of series and $F(\omega)$ is the normalized spectral shape, then the spectrum for series $U^n(t)$ has the shape:

$$S_{U^n}(\omega) = (S_0)^n F(\omega). \tag{2}$$

Ratios (1) and (2) correspond to a simple shift of the spectral curves up or down when power n is greater or smaller than 1, respectively (Figure 4). This result is intuitively clear: the autocorrelation functions for series $U(t)$ and $U^n(t)$ should be similar, at least for a sufficiently small value of n. This intuitive assumption can be proved analytically, and the proper formulas are presented in Appendix A.

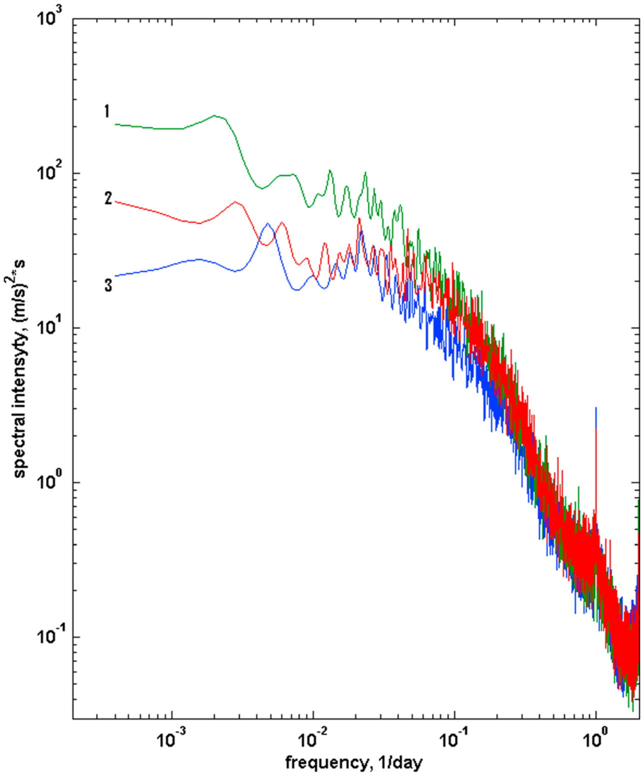

Figure 5. Spectra for wind components $S_{U_i}(\omega)$ and wind modulus $S_U(\omega)$ at the point (0°N, 63°E). Line 1 (green) is $S_{U_X}(\omega)$, line 2 (red) is $S_{U_Y}(\omega)$, and line 3 (blue) is $S_U(\omega)$.

3.3.2. The Spectra for Components and Modulus of a Vector Series

By using the property of section 3.3.1 described above, it is easy to prove that the spectral shapes $S_U(\omega)$, $S_{U_X}(\omega)$, and $S_{U_Y}(\omega)$, estimated for series of the velocity vector, $\mathbf{U}(t) = (U_x(t), U_y(t))$, should be similar. The typical result is shown in Figure 5. The fact that the intensity of spectra for wind modulus $S_U(\omega)$ is smaller than the one for $S_{U_X}(\omega)$ and $S_{U_Y}(\omega)$ could be explained by the antiphase variations of wind component (alike the cyclic motion).

3.3.3. The Ratio Between the Spectra of Original and Filtered Series

The filtered series, $U_{\text{pu}}(t)$, is defined as the difference between initial series $U(t)$ and the annual variability series, $U_{\text{an}}(t)$, which is determined by an averaging over the calendar year of the values for initial long-term series $U(t_i)$, made for each observation at a time-moment t_i. Filtered spectra are used to exclude the impact of the long-term annual variability on the initial series spectral shape which simplifies establishing the relationship between spectra of different geophysical quantities (wind speed, pressure, and wave heights). The typical results of corresponding calculations are shown in Figure 6, leading to the following conclusions:

First, the spectrum for filtered series preserves the spectral shape of initial series in the range of periods from 1 to 100 days. Second, the spectrum of filtered series has the intensity of isolated peaks radically reduced (1 year, 1 day, and their harmonics) that allows spectral slopes and proper frequency ranges for filtered series to be estimated more accurately. Third, the spectrum of the annual variability series, $S_{\text{an}}(\omega)$, retains the spectral shape of original series in the range of periods from 1 to 30–50 days.

Further, we shall actively use the second property, comparing the spectra of different physical quantities.

4. Dynamics Equations and Relationships Between Spectra of Different Quantities

4.1. The Wind Speed Spectra

To clarify the nature of wind speed spectra formation, it is quite natural to consider the Navier-Stokes equations [*Pedlosky*, 1982; *Monin and Yaglom*, 1971], written in the form

$$\frac{\partial U_i}{\partial t} + U_j \frac{\partial U_i}{\partial x_j} + s_i 2\Omega \sin(\varphi) U_j = -\nabla_i P + \text{visc.terms} \tag{3}$$

where $U_i(x,y)$ is the *i*th component of wind speed at the standard horizon z at geographic point (x,y), summation is implied for the repeated subindexes, *i*, *j*, each of which has values *x* and *y*, with the proviso that $i \neq j$ at the Coriolis term; the symbol s_i has values $s_x = 1$, $s_y = -1$ in accordance with the Coriolis force term formulation; the value $\Omega = 7.3 \times 10^{-5}\ \text{s}^{-1}$ is the Earth's angular velocity, and ϕ is the latitude of the point on the Globe. The term $\nabla_i P$ is the *i*th gradient component of pressure field $P(x,y)$, taken at relevant horizon *z* and normalized by the air density. The terms of the viscous forces are written in an implicit form because they are

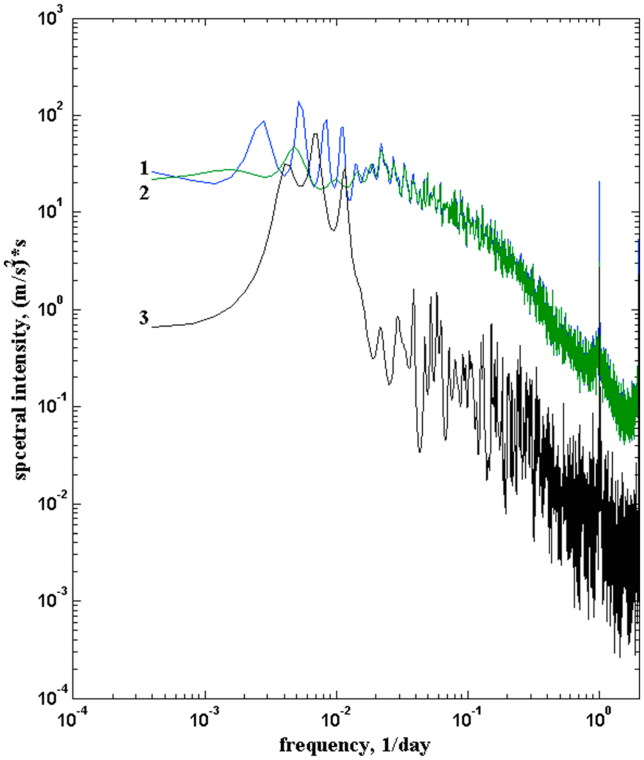

Figure 6. Three types of spectra for wind speed at the point (0°N, 63°E). Line 1 (blue) is the spectrum of initial series, line 2 (green) is the spectrum of filtered series, and line 3 (black) is the spectrum of annual variation series.

considered immaterial due to turbulent character of the flow (i.e., large Reynolds numbers). Furthermore, we consider the simplified form of equation (3) in the form

$$\frac{dU_i}{dt} = F_U \approx -\nabla_i P - \tilde{\Omega}_i U_j, \qquad (4)$$

where the obvious changes of notations are used.

The most important feature of equation (4) is the following: the temporal derivative of wind velocity takes place on the left-hand side, while the right-hand side means the external forcing, F_U. Obviously, the forcing is responsible for the wind-velocity vector evolution, $U(t)$, and, hence, for the spectral shapes of wind speed components. A certain form of equation (4) depends on both the location of the point (x,y) on the Globe and the considered scales of circulation. Options for equations (4) representation are as follows.

First, near the equator, the term of Coriolis force $\widetilde{\Omega}_i U_j$ becomes very small, i.e., the condition is fulfilled:

$$\left|\widetilde{\Omega}_i U_j\right| << |dU_i/dt|, |\nabla_i P|. \qquad (5)$$

The Coriolis force variance with the geographic latitude is the reason of the empirical partition of the latitudes domain into two zones, Z1 and Z2, where the wind-velocity spectra have different shapes.

Second, under condition (5), valid in the zone Z1, the balances of terms in equations (4) are as follows.

Case 4.1.1. If the values of pressure gradient and velocity derivative are comparable, $|\nabla_i P| \cong |dU_i/dt|$,, equation (4) assumes the form

$$\frac{dU_i}{dt} \approx -\nabla_i P. \qquad (6)$$

In this case, the spectrum of wind components, $S_{U_i}(\omega)$, is determined by the spectrum of the same components of pressure gradient, $S_{\nabla_i P}(\omega)$, via the ratio

$$S_{U_i}(\omega) = S_{\nabla_i P}(\omega)/\omega^2, \qquad (7)$$

which follows the formulas for the Fourier transform. Here we neglect the advective terms of the time derivative in equations (6), for simplicity.

From (7) it follows that if the spectrum of the pressure-gradient component, $S_{\nabla_i P}(\omega)$, has the shape of the white noise spectrum in some frequency range, then in the same range, the spectrum slope $S_{U_i}(\omega)$ appears to be equal to -2. According to property in section 3.3.2 described above, the spectra for wind magnitude will have the same slope (in the same period's range). The said provides interpretation of feature Z1–U1 for the wind spectrum.

An example of 4.1.1 case is shown in Figure 7, where the filtered spectra for wind components are compared with filtered spectra for components of the "normalized" pressure gradient. The latter is determined by value $S_{\nabla_i P}(\omega)/\Omega^2$, and further, the notation $\hat{P} \equiv P/\Omega$ is used.

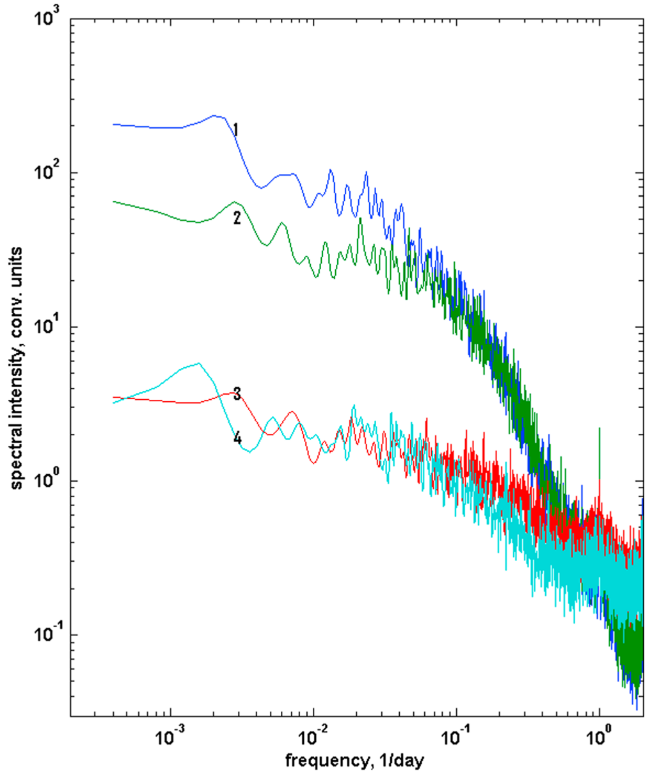

Figure 7. Comparison of the spectra for velocity components U_X, U_y and for components of normalized pressure gradient $\nabla_i \hat{P}$ at the point (0°N, 63°E) (the Z1 zone). Line 1 (blue) is spectrum $S_{U_X}(\omega)$, line 2 (green) is spectrum $S_{U_Y}(\omega)$, line 3 (red) is spectrum $\hat{S}_{\nabla_X P}(\omega)$, and line 4 (light blue) is spectrum $\hat{S}_{\nabla_Y P}(\omega)$.

It is seen that in the range of periods less 2–3 days, we have the case 4.1.1, indeed. A more detailed analysis is given in section 6.

Case 4.1.2. Assume now that the pressure gradient is small compared to the time derivative of wind speed, i.e., consider the situation

$$\left|\widetilde{\Omega}_i U_{\mathrm{j}}\right|, \left|\nabla_i P\right| << \left|\mathrm{d}U_i/\mathrm{d}t\right|. \qquad (8)$$

Then equation (4) degenerates into the equation for stationary turbulent flow

$$\mathrm{d}U_{\mathrm{i}}/\mathrm{d}t \approx 0. \qquad (9)$$

In the case of free atmospheric circulation pattern with high Reynolds numbers, considered here, such a situation is fully consistent with the Kolmogorov-Obukhov (KO) turbulence [*Monin and Yaglom*, 1971]. This assumes that the wind speed spectra with decay law $-5/3$ is expected. Such spectra are observed in the Z1 zone of latitudes and the R2 range of periods, mentioned as the feature Z1–U2. In the literature [*Hamilton et al*., 2008; *Skamarock et al*., 2014; *Monin and Sonechkin*, 2005] such spectra are classified as "the inverse cascade spectra" of the KO type, corresponding to a constant kinetic energy flux to the lower frequencies, produced by the processes of baroclinic instability, taking place at synoptic periods of several days [*Monin and Sonechkin*, 2005].

One can see from Figure 7 that in a wide range of periods, starting from three or more days (R2 range), spectra $S_{\nabla_i P}(\omega)/\Omega^2$ are very small compared to the spectra of wind components, $S_{U_i}(\omega)$. This fact suggests that, in the R2 range, condition (8) is valid, which prompts us to identify the feature Z1–U2 as a manifestation of the KO turbulence.

Case 4.1.3. On the larger time scales (greater than 30–50 days) the turbulent eddies generated by sources of baroclinic instability could be exhausted and totally destroyed, which stops the inverse KO-cascade noted above. Then, as pointed in *Monin and Sonechkin* [2005], "on the scale of a season to a year, the atmospheric dynamics is set up of such a kind that all meteorological quantities have a spectral plateau.". This spectral plateau is referred here as the white noise spectrum. Realization of such a situation is confirmed in Figure 7 for the range of variability scales from 30 days to a year.

Apparently, the atmospheric dynamics on the scales more than 30–50 days, specified in *Monin and Sonechkin* [2005] and *Lovenjoy and Schertzer* [1985], explains feature Z1–U3 realized in the R3 range of periods. It is also important to note that due to the global nature of the atmosphere dynamics in the R3 range, the considered case is realized both near the equator and away from it. Therefore, the conditions (5) and (8) validity is not essential here.

Consider now a modification of equations (4) in the off-equatorial zone Z2.

Case 4.1.4. In the Z2 zone, it is natural to assume realization of the condition

$$\left|\widetilde{\Omega}_i U_{\mathrm{j}}\right|, \left|\nabla_i P\right| >> \left|\mathrm{d}U_i/\mathrm{d}t\right|, \qquad (10)$$

which assumes the geostrophic balance. Then, equation (4) takes the form$_{\mathrm{s}}$

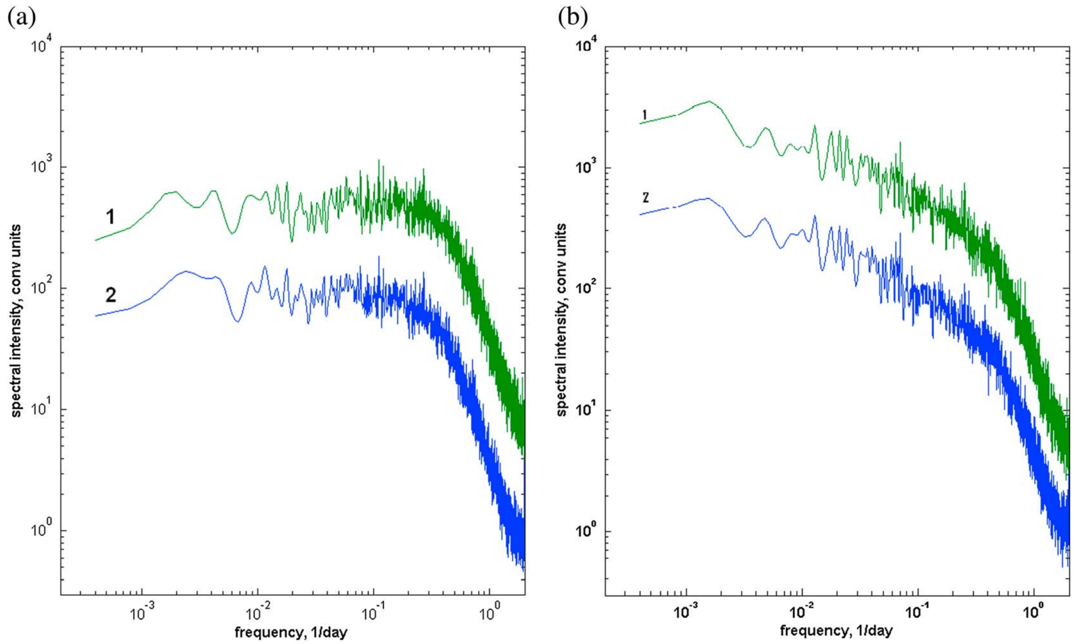

Figure 8. Comparison of the spectra (a) for wind component U_y and for component of normalized pressure gradient $\nabla_X\hat{P}$ and (b) for wind component U_x and for component of normalized pressure gradient $\nabla_Y\hat{P}$ at the point (60°S, 63°E) (the Z2 zone). Lines 1 (green) are pressure-gradient spectra; lines 2 (blue) are wind component spectra.

$$\widetilde{\Omega}_i U_j \approx -\nabla_i P. \tag{11}$$

From equations (11), it is clear that the spectrum of the *j*th component of wind velocity is proportional to the spectrum of the *i*th component of normalized pressure gradient, i.e.,

$$S_{U_j}(\omega) \propto S_{\nabla_i P}(\omega)/\Omega^2. \tag{12}$$

This relationship between spectra for wind speed and pressure-gradient components is fully confirmed with our calculations' results, part of which is shown in Figures 8a and 8b. Thus, all the features of spectral shapes for the wind speed magnitude, described in section 3.1 for the Z2 latitudinal zone, are directly determined by the spectral shape for the pressure-gradient components.

This completes the issue of interpretation the shapes of wind speed spectrum $S_U(\omega)$.

4.2. The Wave Height Spectra

To describe dynamics of formation the spectra for series of significant wave height, $H_s(t)$, we consider the evolution equation for the energy spectrum of surface elevation, which could be written in the form [*Efimov and Polnikov*, 1991; *Komen et al.*, 1994]

$$\frac{\partial S}{\partial t} + (\nabla_{\mathbf{k}}\sigma(k)\nabla_{\mathbf{x}}S) = F_S \equiv NL(S, \mathbf{k}) + IN(\mathbf{U}, S, \mathbf{k}) - DIS(\mathbf{U}, S, \mathbf{k}). \tag{13}$$

Here $S \equiv S(\mathbf{k}; x, y, t)$ is the field of two-dimensional spatial energy spectrum of surface elevation (wind waves), $\sigma(k)$ is the dispersion relation connecting the frequency of gravity waves, σ, with its wave vector, k. Further, the kind of relation $\sigma(k)$ is not essential, but it is important to note that the wave number, k, and the corresponding frequency, σ, used in $\sigma(k)$ and in wave spectrum $S(k)$, are not related to frequency ω used in wave height spectra $S_{Hs}(\omega)$ calculated for the long-term series of significant wave height, $H_s(t)$.

Note that in equation (13), the left-hand side is the total time derivative of spectrum $S(k)$, and the right-hand side is the forcing, F_S. Thus, the analogy between equations (3) and (13) is evident. Therefore, forcing F_S is represented in the form of three well-known terms: (1) The NL-term, describing the nonlinear transfer of wave energy through spectrum $S(\mathbf{k})$; (2) the IN-term, responsible for the energy transfer from the wind to waves;

and (3) the DIS-term, responsible for the rate of wave-energy dissipation [*Efimov and Polnikov*, 1991; *Komen et al.*, 1994].

To determine the equation for significant wave height H_S from equation (13), one could use the known ratio

$$H_S{}^2 = 16\int S(\mathbf{k})d\mathbf{k} = 16\mathrm{E}, \tag{14}$$

where E is the wave-energy density per unit area, normalized by the density of water and the acceleration due to gravity, g. After integration (13) over the wave numbers and neglecting (for simplicity) the advective terms, one could obtain the sought equation for H_S of the form

$$\frac{\partial H_S^2}{\partial t} = \int F_S d\mathbf{k} \propto \mathrm{fun1}(U, \ldots), \tag{15}$$

where fun1 is the result of integrating forcing function $F_S(U, S, k)$ over wave vector $\mathbf{k}$.

Estimate now term fun1 as a function of wind U. For this purpose we take into account the conservative feature of the nonlinear term NL, providing a zero for the integral of NL over $\mathbf{k}$, and semi-empirical feature of parameterizations for terms IN(U,S,$\mathbf{k}$) and DIS(U,S,$\mathbf{k}$) [*Komen et al.*, 1994]. The latter means that functions IN(U,S,$\mathbf{k}$) and DIS(U,S,$\mathbf{k}$) are rather arbitrary. Therefore, following a main physical assumption [*Polnikov*, 2012], we could use the direct proportionality between IN and DIS terms and proportionality of IN-term to the horizontal flux of kinetic energy of the wind, i.e., the ratio: IN ~ U^3 [*Phillips*, 1985; *Polnikov*, 2012]. Then, from (15) we derive

$$\frac{\partial H_S^2}{\partial t} = \int F_S d\mathbf{k} \propto U^3 \times \mathrm{fun2}, \tag{16}$$

where fun2 is the new function of parameters used in functions IN(U,S,$\mathbf{k}$) and DIS(U,S,$\mathbf{k}$), the form of which is not important here. It is essential only that fun2 does not depend on wind U.

By analogy with the transition from equation (6) and (7), it follows from (16) the sought relation between spectra for wave height and wind speed of the form

$$S_{H_S^2}(\omega) \propto S_{U^3}(\omega)/\omega^2, \tag{17}$$

where $S_{U^3}(\omega)$ is the spectrum of the time series for wind speed, taken to the cubic power. Attracting the empirical feature described in section 3.3.1, which states that the spectra of the powered time series is similar to the spectra of linear series, after engaging the first feature for wind spectra, Z1–U1, in the R1 range of scales, we get

$$S_{U^3}(\omega) \propto S_U(\omega) \propto \omega^{-2}. \tag{18}$$

With attracting feature 3.3.1 again, it follows from (17) and (18) that in the considered R1 range of scales, the following ratios must take place:

$$S_{H_S}(\omega) \propto S_{H_S^2}(\omega) \propto S_{U^3}(\omega)/\omega^2 \propto S_U(\omega)/\omega^2 \propto \omega^{-4}. \tag{19}$$

The final part of ratio (19) explains the feature Z1–H1 for wave height spectra in the R1 range.

In the same manner, one can also obtain an interpretation of feature Z1–H2 for spectrum $S_{H_S}(\omega)$, valid in the R2 range of periods. Considering the peculiarity Z1–U2 for wind spectrum and ratios (19) for the wave height spectrum, we get

$$S_{H_S}(\omega) \propto S_U(\omega)/\omega^2 \propto \omega^{-3.7}. \tag{20}$$

Result (20) explains the feature Z1–H2 for the slope of wave height spectra. An explanation of the weaker decay law of spectra $S_{H_S}(\omega)$ in the R2 range of scales (named as the Z1–H2a in section 3.2) requires other physics. It could be the following.

On time scales longer than a few days, waves can reach a fully developed state. In this case, the dynamic equation (13) degenerates to the identity: 0 = 0. Therefore, to get an interpretation of spectral shape for $S_{H_S}(\omega)$, one needs to apply the so-called "fully developed wave" approach, based on the direct-fetch consideration [*Efimov and Polnikov*, 1991; *Komen et al.*, 1994].

According to a simple model of the direct fetch with a constant wind speed U, the dimensionless time, $\widetilde{T}$, defined by formula $\widetilde{T} = tg/U$, should be of the order of 10^5 units, to achieve the fully developed wave state.

This estimate was obtained for values $g = 9.81$ m/s^2 and $U = 10$ m/s. As can be seen, the time of full development for waves is on the order of a day. To consider the wave height spectra, $S_{H_S}(\omega)$, corresponding to the fully developed wave state, it is necessary to consider time scales which are an order larger. These scales correspond to the R2 and R3 spectral ranges introduced above.

The dimensionless energy of the fully developed wave, defined by the formula

$$\widetilde{E} = \left(H_S^2/16\right)g^2/U^4, \tag{21}$$

reaches a fixed value of the order of $\widetilde{E} \approx (4-5)10^{-5}$ [*Efimov and Polnikov*, 1991]. From ratios (21) and (14) it follows that, in this case, the value of wave height, H_S, is related to the value of wind speed U, by the ratio

$$H_S \propto U^2. \tag{22}$$

Using feature in section 3.3.1, we obtain the following ratio:

$$S_{H_S}(\omega) \propto S_{U^2}(\omega) \propto S_U(\omega) \tag{23}$$

which is valid for the fully developed wave state realized on the time scales more than 10 days. Thus, the stated wave state is realized in a part of the R2 range and in the whole R3 range.

Thus, if we keep in mind the feature Z1–U2 for wind spectra, then from ratio (23), in the R2 range of periods we obtain

$$S_{H_S}(\omega) \propto \omega^{-5/3}, \tag{24}$$

while in the R3 range, taking into account the feature Z1–U3, we obtain

$$S_{H_S}(\omega) \propto \omega^{-0} = \text{const}. \tag{25}$$

Accordingly, ratios (24) and (25) provide the sough interpretation both the feature Z1–H2a and feature Z1–H3 for spectra $S_{H_S}(\omega)$, which are valid in the R2 and R3 ranges of periods, respectively.

Thus, the interpretation of spectral shapes for wave height in zone Z1 is fully completed. Interpretation of the spectral shapes $S_{H_S}(\omega)$ in the zone Z2 is directly follows from the same ratios, (19) and (23).

5. Detailed Interpretation of the Spectra in the D1 Domain of Scales

This section contains some explanations of how to use the above ratios for interpretation features of the spectral shapes for wind speed, $S_U(\omega)$ and wave height, $S_{H_S}(\omega)$, in the D1 domain.

To check the applicability of the result found in section 4, calculations of the spectra for components of pressure gradient have been executed. To this end, the data for pressure field were extracted from the ERA-Interim reanalysis with resolution 0.75 × 0.75°, permitting us to calculate accurately pressure gradients at the given set of geographic locations (Figure 1). Representative spectra for components of normalized pressure gradient, $S_{\nabla_i P}(\omega)/\Omega^2$ are shown in Figures 7 and 8a and 8b in comparison with the spectra for wind-velocity components, $S_{U_i}(\omega)$. With the aim of a clearer comparison, calculations of spectra $S_{\nabla_i P}(\omega)$ and $S_{U_i}(\omega)$ were done for the filtered series of components, both wind velocity, and pressure gradient.

After that, a check was carried out for feasibility of conditions (5), (8), or (10). In this case, the problem of comparison of intensities of spectra $S_{U_i}(\omega)$ and $S_{\nabla_i P}(\omega)$ is raised, provided by the difference of their dimensions. Such a comparison is needed for the estimation of the extent of smallness of the pressure gradient. This problem was solved by introducing the spectra of the so-called normalized pressure gradient, $\hat{S}_{\nabla_i P}(\omega)$, defined by the formula

$$\hat{S}_{\nabla_i P}(\omega) = S_{\nabla_i P}(\omega)/\Omega^2 \equiv S_{\nabla_i \boldsymbol{P}}(\omega). \tag{26}$$

Justification of using this type of normalization follows from the geostrophic balance equation (11).

It was empirically found that if the value of spectrum $\hat{S}_{\nabla_i P}(\omega)$ exceeds the value of $S_{U_i}(\omega)$, then cases 4.1.1 or 4.1.4 are realized, and the pressure gradient should be taken into account. Otherwise, case 4.1.2 takes place. All possible ratios between values of spectra $\hat{S}_{\nabla_i P}(\omega)$ and $S_{U_i}(\omega)$, mentioned above in section 4, are well demonstrated in Figures 7 and 8a and 8b. From Figure 7, it is seen that in the near-equator latitude zone, Z1, and the range of periods less than 2–3 days (the R1 range), the ratio between intensities of spectra $\hat{S}_{\nabla_i P}(\omega)$ and $S_{U_i}(\omega)$ correspond to condition (5) and using of formula (7) (the case 4.1.1). Thus, in the R1 range, the spectrum of filtered pressure gradient has a slope close to -0, and formula (7) leads to the wind-velocity components spectra of the form $S_{U_i}(\omega) \propto \omega^{-2}$. The subsequent using the property 3.3.2 provides the completion of treatment feature Z1–U1 for the wind-velocity modulus spectrum.

Furthermore, from Figure 7 it is seen that in the R2 and R3 range of periods, the spectra for components of normalized pressure gradient become small in comparison with the wind-components spectra, i.e., the case 4.1.2 is realized. Note that in the R2 range, such a situation is valid in the whole zone Z1, and, in this range of periods, the spectra for wind components are of the KO type. But in the R3 range the case 4.1.3 takes place, and the spectra for wind have a plateau (slope is equal to -0), which is valid in both zones, Z1 and Z2. The latter is due to the fact that on the scales from seasons to a year, the dynamics of atmosphere is determined by global processes rather than local ones [*Monin and Sonechkin*, 2005].

In the zone Z2, the spectra for components of normalized pressure gradient become greater than spectra for wind-velocity components (Figures 8a and 8b), i.e., condition (10) is valid, and the case of geostrophic balance is realized (the case 4.1.4).

It is left to add that according to the theory presented in section 4.2, all the features of spectra for wave height $S_{H_S}(\omega)$ are uniquely defined by the features of wind speed spectra $S_U(\omega)$ via ratios (19) and (23). This is manifested by a curve-to-curve comparison of proper spectra $S_{H_S}(\omega)$ and $S_U(\omega)$ presented in Figures 2 and 3, including the range where spectra have a plateau (the R3 range).

Clearly, some small deviations from theoretical ratios (19) and (23) could take place in real relations between slopes in spectra $S_{H_S}(\omega)$ and $S_U(\omega)$. They are fully determined by both the adopted theoretical approximation (neglecting the advective part in time derivative) and a sample variability of the statistical estimates for spectral slopes. We believe that establishing more correct theoretical relationships is impossible, and there is no alternative to ratios (19) and (23). In addition, it should be noted that the statistical errors for spectra estimates (and for their slopes), as was mentioned in section 2, are of the order of 10–15%. Therefore, in our opinion, the visible slight deviations between the empirical slopes in Figures 2 and 3 and proper theoretical ratios (19) and (23) do not reduce the significance of the presented treatments for the spectral shapes $S_{H_S}(\omega)$ and $S_U(\omega)$ proposed in this paper.

6. The Spectra of Wind and Waves in the D2 Domain of Scales

With the aim of studying the scales for wind field and wavefield variabilities in the D2 domain (variability periods from 1 to 15 years), we estimated their spectra by using the same 6-hourly series smoothed by 15 day averaging. Representative results are shown in Figures 9a and 9b and 10a and 10b. Analysis of them leads to the following conclusions.

First, in the D2 domain there is no united set of isolated frequencies of both meridional and zonal sections. This is valid for all the considered variables: wind, pressure, and wave height. The observed mixed spatial variability of the isolated scales indicates the absence of global dynamics of atmosphere and wind waves throughout the IO as a single system. This result confirms our previous conclusion that the whole IO is shared in a set of areas (spatial zones) with independent dynamics of the atmosphere [*Pogarskii et al*., 2012].

Second, the observed smoothed peaks of isolated frequencies, marked in Figures 9 and 10 by digits, have the intensity of 2–3 orders lower than the annual one (right-most marked frequency). It is well seen in Figures 9b and 10a and 10b, where the spectra are built for the initial series (in Figure 9a, the spectra are shown for series filtered from the annual variation). This result is quite expected since the amplitude of annual variability for geophysical quantities should be much greater than the long-term variabilities [*Monin and Sonechkin*, 2005].

At the same time, the smallness of amplitudes for the multiyearly peaks does not allow us to assert that the spectra of considered series can be represented as a discrete set of individual harmonics, as noted in *Serykh and Sonechkin* [2015]. Apparently, to confirm the assumption of a discrete set of harmonics, allocated in the D2 domain, it is necessary to use much longer series (100 years or more), as it was done in *Serykh and Sonechkin* [2015].

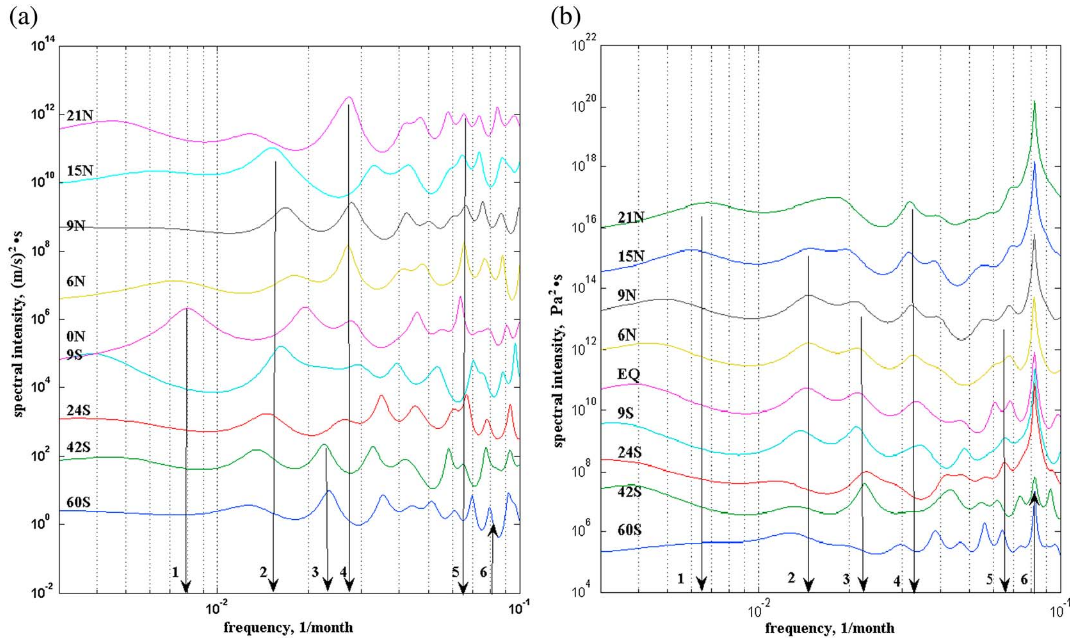

Figure 9. Climatic spectra: (a) wind speed (filtered series) and (b) pressure (initial series), at nine points on 63°E section. Spectra are shifted up by a factor of 30.

Third, peaks marked with digit 2 preserve the best constancy among all the visible maxima observed in the spectra calculated. They correspond approximately to the variability scale of 60–70 months (about 5.5 years), which was also observed in *Serykh and Sonechkin* [2015]. It can be considered as the second harmonic of the known 11 year solar cycle, or as a response to the Indian Ocean dipole or El Niño–Southern Oscillation phenomena having the same periodicity [*Stopa and Cheung*, 2014]. The peaks marked by digits 3 and 4 correspond apparently to the third and fourth harmonic of the same cycle (though, they do not correspond well to the aforementioned, especially in Figure 9a). At the same time, the 11-yearly harmonic, corresponding to the cycle of solar activity, is virtually absent in our calculations. Apparently, it is due to the small length of data series (about 3 cycles only) and the noise of accidental variability of this natural phenomenon. Additionally, disadvantages of the reanalysis used could play some smoothing role. Therefore, this result is important as an indication of the prospects for further research in this direction.

In conclusion, we should note that the results presented here emphasize the necessity to continue such studies in the future, based on extended reanalysis because a lot of mentioned issues are the matters of considerable interest in geophysics, and they are still far from being resolved.

7. Conclusion

The results presented above give extensive new information about the nature of temporal variability for wind and wavefields, the features of their long-term spectra, the scales of their temporal variability, and their spatial variability in the IO. The list of main results is the following.

We have shared the scales of variability into two domains of periods, D1 and D2, in which the tasks of spectra investigation are different. In the D1 domain, covering periods from half a day to a year, the spectra of geophysical quantities are continuous. Here the main interest is a clarification of mechanisms responsible for spectra slopes formation, which could be different in the different latitudinal zones and different frequency ranges, denoted in this work as the zones Z1 and Z2 and ranges R1, R2, and R3, respectively (section 3). In the D2 domain, covering periods from a year to 15–20 years, the spectra of the same quantities, according to *Serykh and Sonechkin* [2015], are expected to be discrete ones. Here the main interest is to clarify the issue of unity for a set of distinguished discrete harmonics, valid in the whole IO as a single system. In this paper, all these points were considered and solved based on the wind field from the ERA-Interim reanalysis for 1979–2015 years and the wavefield calculated earlier with the modified wind-wave model WAM [*Samiksha et al*., 2015].

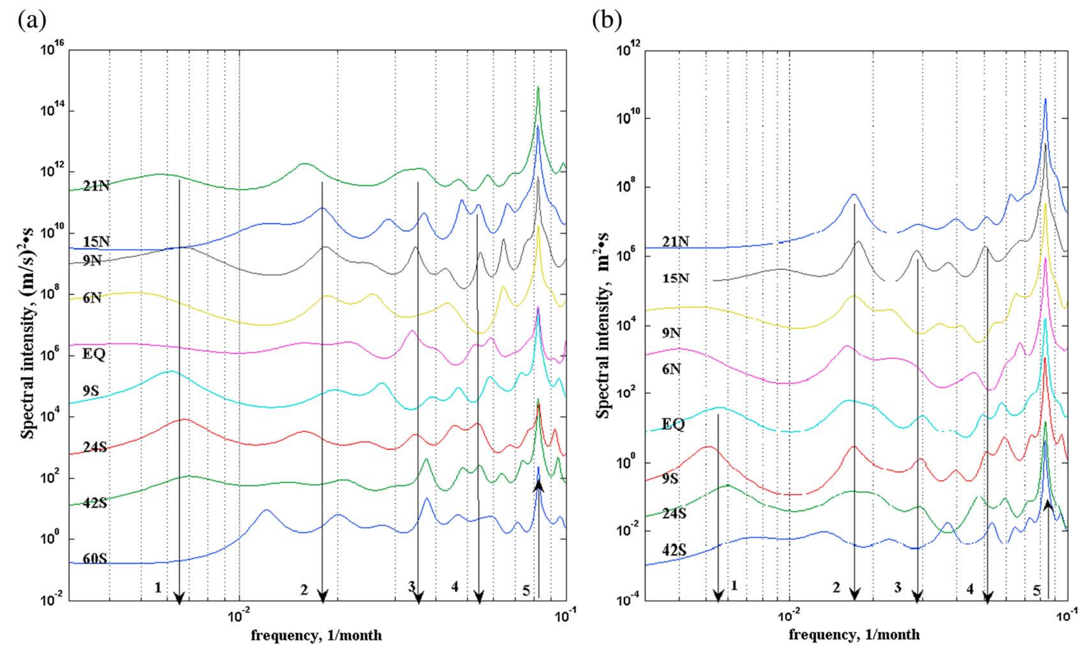

Figure 10. Climatic spectra: (a) wind speed and (b) wave height, at nine points on 90°E section (initial series). Spectra are shifted up by a factor of 30.

In the D1 domain of scales, the empirical temporal spectra for wind and waves, $S_U(\omega)$ and $S_{H_s}(\omega)$, were described in two latitudinal zones Z1 and Z2 (section 3), and interpreted in the three ranges of periods R1 R2, and R3 (sections 4 and 5). Some auxiliary results useful to further analysis were found, describing the relations between spectra of the powered series, spectra for modulus and components of a vector quantity, and spectra of original and filtered series (section 3.3).

Based on analysis of the Navier-Stokes equations, the original version of theoretical description of spectra formation mechanisms for the spectra of wind speed components was presented in section 4. It was shown the deep and physically justified relationship between the wind speed spectra and the spectra for pressure-gradient components. Herewith, the nature of Coriolis-force impact on the shapes of wind speed spectra has been identified. The nature of relationship between the spectra for wave height and wind speed was clarified based on analysis of the evolution equation (13) for the energy spectra of wind waves (section 4.2). Consequentially, the obtained theoretical results have allowed completing the interpretation of spectral shapes for wind speed and wave heights, obtained from empirical calculations in the D1 domain of periods (section 5). The task of continuation of such a study was set up, based on the proposal of using a more complete and accurate database gathered by all the modern observation and modeling techniques mentioned in section 1.

The results of spectra calculations in the D2 domain of scales are as follows. (1) It was established the absence of a united set of discrete scales of variability for both the atmospheric circulation and wavefield in the IO is a single system. (2) In our case, the spectra of series considered cannot be represented as a set of individual harmonics. (3) The only repeated distinguished scale of 5.5 years was found in the spectra for considered data. Therefore, the problem of studying shapes of the spectra for fields of wind, pressure, and wind waves in the D2 domain is transferred to the prospect of further research. At present, such a research has an even greater degree of importance than one in the D1 domain, for which the basic issues of interpretation the spectral shapes for hydrometeorological fields can be regarded as resolved.

Finally, according to the results of *Tsuchiya et al*. [2011] and *Polnikov and Pogarskii* [2013], the modeled series of geophysical quantities provided by numerical simulations have the same spectral shapes as observed ones. In our paper [*Kubryakov et al*., 2016], a good agreement was shown for a 1 year history of the altimeter and simulated data. This encouraging fact allows us to hope that spectral shapes of long-term series are similar to ones for measured and simulated quantities. In the future, this issue should be studied in detail by means of collecting the proper long-term satellite data.

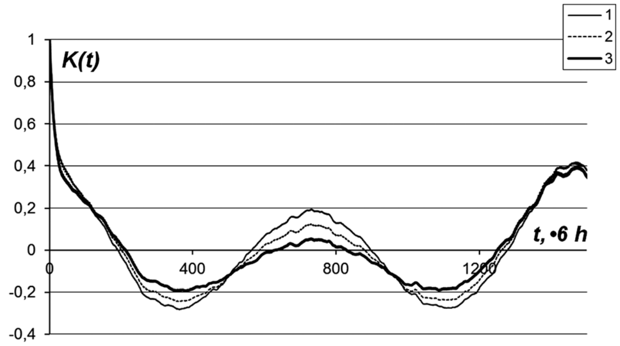

Figure A1. The normalized correlation function $K_{A^n}(j)/D^n$ of the powered series for wind speed at the point (0°N, 63°E). 1 = {$U(t)$} series, 2 = {$U(t)^2$} series, and 3 = {$U(t)^3$} series.

Appendix A: Similarity of the correlation functions for the powered time series

Let us show analytically a similarity of correlation functions for the powered time series. This appendix is presented by the request of reviewer, as it is a very interesting point.

Denote the original series with the zero mean value as {A_i}, where $i = 1, 2, \ldots, N$ is the number of term A_i, and N is the length of series. The correlation function $K_A(j)$ of series {A_i} has the form

$$K_A(j) = \frac{1}{N-j}\sum_{i=1}^{i=N-j} A_i A_{i+j} = \frac{\Delta^2}{N-j}\sum_{i=1}^{i=N-j}(A_i/\Delta)\left(A_{i+j}/\varDelta\right) = \frac{D}{N-j}\sum_{i=1}^{i=N-j}\widetilde{A}_i\widetilde{A}_{i+j}, \qquad \text{(A1)}$$

where j is the shift of correlation, $\varDelta$ is the standard deviation of the series, D is its dispersion, and $\tilde{A}_i = A_i/\varDelta$ is the normalized term of series. Let us introduce the following notation:

$$\widetilde{A}_i = A_i/\Delta = \pm(1-\varepsilon_i) \qquad \text{(A2)}$$

where signs $\pm$ correspond the sign of term A_i. It is obvious that for overwhelming numbers of i, the condition $|\varepsilon_i| < 1$ is valid, and the sum of the terms in (A1), corresponding to the cross productions, $\varepsilon_i\varepsilon_{i+j}$, is very small due to a randomness of variables ε_i. Then, in the linear approximation for the smallness of ε_i, correlation coefficient $K_A(j)$ gets the form

$$K_A(j) = \frac{\pm D}{N-j}\sum_{i=1}^{i=N-j}(1-\varepsilon_i)\left(1-\varepsilon_{i+j}\right) \cong \pm D\left[1 - \frac{1}{N-j}\sum_{i=1}^{i=N-j}\left(\varepsilon_i + \varepsilon_{i+j}\right)\right] = \pm D\left(1-\phi_j\right). \qquad \text{(A3)}$$

In (A3) the presentation for $K_A(j)$ is to be read separately for each sign of coefficient $K_A(j)$, and ϕ_j is the deviation of the normalized correlation coefficient, $K_A(j)/D$, from its limiting values equal to ± 1. It is evident that for the fixed sign of $K_A(j)$, the ratio $0 \le \phi_j \le 1$ is true.

Now for the series to nth power, consisting of terms A_i^n, with accounting ratios (A1) and (A3), in the linear approximation for smallness of ε_i, we obtain

$$K_{A^n}(j) = \frac{\pm D^n}{N-j}\sum_{i=1}^{i=N-j}(1-\varepsilon_i)^n\left(1-\varepsilon_{i+j}\right)^n \cong \pm D^n\left[1 - n\phi_j\right]. \qquad \text{(A4)}$$

From (A4) it follows that for different powers n, the normalized coefficients, $K_{A^n}(j)/D^n$, differ ones from the others by the degree of deviation from the limiting values, ± 1, only (for the relatively small values of n and ϕ_j). It means that the shapes of correlation functions are similar for different powered series (in each range having a fixed sign of $K_{A^n}(j)$, separately). The said is well illustrated in Figure A1. From Figure A1 it is evidently seen the real similarity of $K_{A^n}(j)/D^n$ functions for $n = 1, 2, 3$ values, obtained by the exact calculations, on the example of wind speed series at point (0°N, 63°E). This finalizes the posed task.

Acknowledgments
The authors are grateful to Efimov V.V. for information about paper [*Tsuchiya et al.*, 2011] and to academician Golitsyn G.S. for the opportunity to get acquainted with his book [*Golitsyn*, 2013] in advance, and for preliminary discussion of the results. We also thank P.F. Demchenko, D. G. Chechin, and D. M. Sonechkin for their helpful comments and recommendations and V. G. Perepelkin for his advice on using the spectral analysis software. This work was supported by the RFBR project 15-55-45106-IND_a in the part of calculations, and by the RSF project 14-27-00134 in the part of analysis.. The wind data used can be found in *Berrisford et al.* [2011] (http://apps.ecmwf.int/datasets/data/interim-full-daily/levtype=sfc/). The wave data were computed by us with the modified version of model WAM4, described in *Polnikov* [2005] and [*Samiksha et al.* [2015]. There is no proper open database.

References

Berrisford, P., D. Dee, P. Poli, R. Brugge, K. Fielding, M. Fuentes, P. Kallberg, S. Kobayashi, S. Uppala, and A. Simmons (2011), *The ERA-Interim archive version 2.0, ERA Report Series 1*, ECMWF, Shinfield Park, Reading, U. K.

Efimov, V. V., and V. G. Polnikov (1991), *Numerical Modeling of Wind Waves*, "Naukova Dumka" publishing house, Kiev.

Golitsyn, G. S. (2013), *Statistics and Dynamics of Natural Processes and Phenomena*, pp. 398 , "Krasand" publishing house, Moscow.

Govindau, R. H., D. Viushiu, A. Bunde, S. Brenner, S. Havlin, and H.-J. Schellnhuber (2002), Global climate models violate scaling of the observed atmospheric variability, *Phys. Rev. Lett.*, *89*, 28,501–28,504.

Gulev, S. K., and V. Grigorieva (2006), Variability of the winter wind waves and swell in the North Atlantic and North Pacific as revealed by the voluntary observing ship data, *J. Clim.*, *19*, 5667–5685.

Hamilton, K., O. Y. O. Takahashi, and W. Ohfuchi (2008), Mesoscale spectrum of atmospheric motions investigated in a very fine resolution global general circulation model, *J. Geophys. Res.*, *113* D18110, doi:10.1029/2008JD00978.
Komen, G. J., L. Cavaleri, M. Donelan, K. Hasselmann, and P. A. E. M. Janssen (1994), *Dynamics and Modelling of Ocean Waves*, pp. 532 , Cambridge Univ. Press.
Kubryakov, A. A., V. G. Polnikov, and F. A. Pogarskiy (2016), Comparing numerical and satellite data of wind wave fields in the Indian Ocean, *Russ. Meteorol. Hydro.*, *41*, 130–135.
Lorenz, E. N. (1991), Dimension of weather and climate attractors, *Nature*, *353*, 241–244.
Lovenjoy, S., and D. Schertzer (1985), Scale invariance in climatological temperatures and the spectral plateau, *Ann. Geophys.*, *2*, 401–410.
Monin, A. S., and A. M. Yaglom (1971), *Statistical Fluid Mechanics: Mechanics of Turbulence*, vol. 2, pp. 720 , The MIT Press, Cambridge.
Monin, A. S., and D. M. Sonechkin (2005), *Climate Oscillation*, pp. 192 , "Nauka" Publ. house, Moscow.
Pedlosky, J. (1982), *Geophysical Fluid Dynamics*, pp. 380 , Springer Verlag, Heidelberg-Berlin, New York.
Phillips, O. M. (1985), Spectral and statistical properties of the equilibrium range in wind-generated gravity waves, *J. Fluid Mech.*, *156*, 505–631.
Pogarskii, F., V. Polnikov, and S. A. Sannasiraj (2012), Joint analysis of the wind and wave-field variability in the Indian Ocean area for 1998–2009, *Izv. Atmos. Ocean. Phys.*, *48*, 639–656.
Polnikov, V. G. (1985), Features of the adaptive spectral analysis of hydrophysical processes. Proceedings of the 5th All-Union Conference on Statistical meteorology, Kazan, 146–151.
Polnikov, V. G. (2005), Wind-wave model with an optimized source function, *Izv. Atmos. Ocean. Phys.*, *41*(5), 594–610.
Polnikov, V. G. (2012), Spectral description of the dissipation mechanism for wind waves. Eddy viscosity model, *Mar. Sci.*, *2*, 13–26.
Polnikov, V. G., and F. A. Pogarskii (2013), Short-term variability of wind and waves, based on buoy measurements and numerical simulations in the Hindustan area, *Mar. Sci.*, *3*(2), 48–53.
Samiksha, S. V., V. G. Polnikov, P. Vethamony, R. Rashmi, F. Pogarskii, and K. Sudheesh (2015), Verification of model wave heights with long-term moored buoy data: Application to wave field over the Indian Ocean, *Ocean Eng.*, *104*, 469–479.
Serykh, I., and D. Sonechkin (2015), Evidence of a strange non-chaotic attractor in the El Niño dynamics, *Geophys. Res. Abstr.*, *17*, EGU2015–78.
Skamarock, W. C., S. H. Park, J. B. Klemp, and D. C. Snyder (2014), Atmospheric kinetic energy spectra from global high-resolution. Non-hydrostatic simulations, *J. Atmos. Sci.*, *71*, 4369–4381.
Stopa, J. E., and K. F. Cheung (2014), Periodicity and patterns of ocean wind and wave climate, *J. Geophys. Res. Oceans*, *119*, 5563–5584, doi:10.1002/2013JC009729.
The WAMDI Group (1988), The WAM—A third generation ocean wave prediction model, *J. Phys. Oceanogr.*, *18*, 1775–1810.
Tsuchiya, C., K. K. Sato, T. Nasuno, A. T. Noda, and M. Satoh (2011), Universal frequency spectra of surface meteorological fluctuations, *J. Clim.*, *24*, 4718–4732.
Young, I. R., A. V. Babanin, and S. Zieger (2013), The decay rate of ocean swell observed by altimeter, *J. Phys. Ocean.*, *43*, 2322–2333.
Young, I. R., S. Zieger, and A. V. Babanin (2011), Global trends in wind speed and wave height, *Science*, *332*, 451–455.